Catalysis Today 175 (2011) 133–140

Contents lists available at ScienceDirect

Catalysis Today

journal homepage: www.elsevier.com/locate/cattod

In situ observation of platinum sintering on ceria-based oxide for autoexhaust catalysts using Turbo-XAS

Yasutaka Nagai[a,*], Kazuhiko Dohmae[a], Yasuo Ikeda[b,1], Nobuyuki Takagi[c,1], Naoyuki Hara[b,1], Toshitaka Tanabe[a], Gemma Guilera[d,2], Sakura Pascarelli[d], Mark A. Newton[d], Naoki Takahashi[a], Hirofumi Shinjoh[a], Shin'ichi Matsumoto[e]

[a] TOYOTA Central R&D Labs., Inc., Nagakute, Aichi, 480-1192, Japan
[b] TOYOTA Motor Europe Technical Centre, Zaventem, B-1930, Belgium
[c] TOYOTA Motor Corporation Higashi-fuji Technical Center, Shizuoka, 410-1193, Japan
[d] European Synchrotron Radiation Facility, Grenoble, F-38043, France
[e] TOYOTA Motor Corporation, Toyota, Aichi, 471-8572, Japan

ARTICLE INFO

Article history:
Received 21 October 2010
Received in revised form 9 February 2011
Accepted 28 February 2011
Available online 2 April 2011

Keywords:
Platinum
Sintering
XAFS
Automotive catalyst
Ceria–zirconia
Oxygen storage capacity

ABSTRACT

Using a time resolved X-ray absorption spectroscopy (XAS) technique, we studied an in situ dynamic observation of sintering for Pt particles supported on a ceria-based oxide and Al_2O_3 supports under cyclic oxidizing/reducing conditions at 800 °C. The effect of the support oxide and the amount of Pt loading on the Pt sintering was investigated. The sintering of Pt particles in 2 wt% Pt/ceria-based oxide could be inhibited, when compared to in 2 wt% Pt/Al_2O_3. Moreover, 0.5 wt% Pt and 1 wt% Pt/ceria-based oxide with a lower Pt loading brought higher stability of Pt against sintering. For a 0.5 wt% Pt/ceria-based oxide catalyst, sintering was completely inhibited and highly dispersed Pt particles (particle size; 1.5 nm) were maintained under redox cycling at 800 °C. These results lead to the conclusion that Pt–O–Ce bond formation on the surface of a ceria-based oxide under oxidative conditions in redox cycling inhibits the sintering of Pt particles, and that the Pt–O–Ce anchor site (its strength and number) has an important role in the sintering inhibition of Pt particles on ceria-based oxide. In addition, we note and discuss apparent change in the oxygen storage/release performance of ceria-based oxide from the viewpoint of the Pt particle size and the intrinsic bulk behavior of ceria-based oxide.

1. Introduction

Supported precious metal catalysts such as platinum (Pt)–rhodium (Rh)–palladium (Pd) system have been widely utilized in various industrial catalysts, especially in the automotive converter to abate harmful gas emissions from gasoline- or diesel-driven engines. Since three-way catalysts (TWCs) for gasoline-powered vehicles were commercialized in the USA and Japan in 1977 [1], they have played an important role in the purification of automobile emissions. Recently, in association with growing demands for global environmental protection, various improvements such as high catalytic activity, reduced use of precious metals and increased longevity are demanded for advanced TWCs. One of the major problems for further improvements is the degradation of catalytic activity caused by decreases in metal surface area in supported precious metal catalysts.

Basically, the TWC consists of precious metals such as Pt, Rh or Pd, an inorganic oxide support such as Al_2O_3, and a ceria-based oxide as an oxygen storage component. These precious metals act as the active site to purify harmful automotive emission. The precious metal particles are a few nanometer (nm) in diameter, and are dispersed on the support oxide. When the TWC is exposed to high temperatures, the particle size of the precious metal tends to increases greatly via either particle diffusion/agglomeration or through ripening processes. The result is that the active metals are gradually buried within the bulk of the particle where they can no longer be used to affect the desired chemical conversions that occur on the particle surface. Sintering of the precious metal particles during operation is a major contributor to decreases in the catalytic activity, i.e. degradation [2–5]. As early as 1976 Dalla Betta et al. established thermal sintering as responsible for a 20 fold drop in the available noble metal area and activity in CO and hydrocarbon oxidation in Pt and Pd/Al_2O_3 washcoated monolithic catalysts [6].

Exhaust gases exiting from gasoline engines change quickly and dramatically during operation. Temperatures can rise tran-

* Corresponding author. Fax: +81 561 63 6150.
E-mail address: e1062@mosk.tytlabs.co.jp (Y. Nagai).
[1] Current address: TOYOTA Motor Corporation, Toyota, Aichi, 471-8572, Japan.
[2] Current address: ALBA-CELLS, Bellaterra, Barcelona, Spain.

0920-5861/$ – see front matter © 2011 Elsevier B.V. All rights reserved.
doi:10.1016/j.cattod.2011.02.046

siently to high values in excess of 800 °C in the case of modern car catalysts, and the exhaust gas composition itself fluctuates quickly between oxidative and reductive compositions. Specifically, the activity of Pt supported catalysts decreases significantly after high temperature aging in an oxidative atmosphere due to the sintering of Pt particles compared with that in a reductive atmosphere [2,3]. In our previous study [7], we reported that Pt in 2 wt% Pt/ceria-based oxide did not sinter after aging treatment at 800 °C in air but did markedly sinter in 2 wt% Pt/Al_2O_3. Using Pt L_{III}-edge extended X-ray absorption fine structure (EXAFS) under ex situ condition, we found that the Pt–O–Ce bond (i.e., the Pt–oxide support interaction) acted as an anchor and inhibited the sintering of Pt particles on ceria-based oxide. From the coordination number of Pt–O and Pt–Ce shells estimated from curve-fitting analysis, it could be concluded that this Pt–O–Ce bond was formed at the surface of the support and not in the bulk [7]. A similar Pt–O–Ce surface complex on a ceria-based oxide support was also reported by Diwell et al. and Murrell et al. [8,9]. If this theory is correct, the loading amount of Pt supported on ceria-based oxide would have a significant effect on the sintering behavior of Pt particles, because the number of surface Pt anchor sites is limited.

To verify the Pt anchor effect on Pt sintering, in the current paper, we observe, through the application of in situ and time resolved X-ray absorption spectroscopy (XAS), the dynamics of Pt sintering in Pt/ceria-based oxide supports. We use various amounts of Pt loading, and reproduce in situ conditions of redox cycling at high temperature, to be as close as possible to the real situation of the autoexhaust operation. In the current case, real time observation of changes in the noble metal structure were made at the Pt L_{III}-edge using the fluorescence yield variant (Turbo-XAS) of energy dispersive XAS, developed by Pascarelli et al. at ID24 of the ESRF [10]. The combination of low levels of Pt in the catalysts, with high levels of heavy, absorbing, elements such as Ce and Zr severely compromises the conventional, transmission based, dispersive XAS experiment. Moreover, and to date, Quick Scanning EXAFS has not been shown to fare any better for sample systems such as these for the time resolutions required to study these processes. In order, therefore, to obtain a window into the structural-reactive behavior of Pt in these systems with a suitable time resolution the fluorescence variant has been adopted as it permits Pt L_{III}-edge X-ray absorption near edge structure (XANES) on the required timescale even for these taxing samples [11]. Importantly, this approach allows us to actually observe and quantify the size and loading dependence of both the Pt particle behavior in situ and as it occurs rather than in an ex situ and post mortem manner. In addition, we are also able to obtain a window into how the changes in the average size of the Pt nanoparticles relates to apparent changes (measured using mass spectrometry) in the oxygen storage/release capacity (OSC) of the ceria-based oxide material itself.

2. Experimental

2.1. Catalyst preparation

Pt/Al_2O_3 and Pt/ceria-based mixed oxide (Ce–Zr–Y mixed oxide, referred to as CZY) catalysts were prepared by the following methods. Al_2O_3 as a support oxide was supplied by Nikki Universal Co., Ltd.: its crystal structure was γ-type. CZY powders as a support oxide was prepared using a coprecipitation process with aqueous NH_3 using $Ce(NO_3)_3$, $ZrO(NO_3)_2$ and $Y(NO_3)_3$ in aqueous solutions. The precipitate was dried at 110 °C and calcined in air at 700 °C for 3 h. CZY contains 50 wt% CeO_2, 46 wt% ZrO_2 and 4 wt% Y_2O_3, and its crystal structure was cubic. 2, 1 and 0.5 wt% Pt/CZY and 2 wt% Pt/Al_2O_3 catalysts were prepared by the conventional wet impregnation of CZY and Al_2O_3 powders with $Pt(NH_3)_2(NO_2)_2$ aqueous solution. The impregnated powders were dried overnight at 110 °C and then calcined at 500 °C for 3 h in air.

2.2. Catalyst characterization

The specific surface areas of the samples were estimated using the N_2 adsorption isotherm at −196 °C by the one-point Brunauer–Emmett–Teller (BET) method using an automatic surface analyzer (Micro Sorp 4232II, Micro Data Co., Ltd.). The samples were degassed in flowing N_2 at 200 °C for 20 min.

Powder X-ray diffraction (XRD) experiments were carried out in air at room temperature using a RINT2000 (Rigaku Co., Ltd.) diffractometer with Cu Kα radiation (1.5406 Å). The catalyst powder was pressed into wafers and affixed to standard-sized microscope slides. The Pt catalyst samples were reduced by 5% H_2 (N_2 balance) at 400 °C for 30 min before the XRD measurements.

The average particle size of Pt metal was measured using a CO pulse adsorption method [12]. The catalysts were pre-treated in flowing pure oxygen, and then pure hydrogen at 400 °C. With this reductive treatment of hydrogen, Pt is reduced to Pt metal. CO pulse adsorption was carried out in flowing He at −78 °C. At this temperature, the CO uptake on ceria support was almost entirely suppressed, and CO was adsorbed to only the surface of Pt [13]. The average particle size was calculated from CO uptake assuming that CO was adsorbed on the surface of spherical Pt particles at CO/(surface Pt atom) = 1/1 stoichiometry.

2.3. In situ and dynamics Turbo-XAS/mass spectrometry measurement

Real time observation of the sintering behavior of Pt particles was made by in situ time resolved Turbo-XAS (T-XAS) in fluorescence mode at ID24 (ESRF) [10]. The experimental set-up for the T-XAS and quick gas changing from an oxidative to reductive atmosphere is shown in Fig. S1 in the Supplementary data. In T-XAS, a narrow slit (120 μm wide) is scanned through the polychromatic fan of radiation downstream of the crystal, selecting a monochromatic beam. Incoming X-rays (I_0) and fluorescence X-rays (I_1) were recorded by two Si-diode detectors. The I_0 diode was placed perpendicularly with respect to the beam, and the I_1 diode was placed facing the sample and oriented perpendicular to the incident beam direction in order to minimize elastically scattered radiation. The sample (60 mg) was pressed to a disk (5 mmϕ) and placed in an in situ cell equipped with a rapid gas switching system, allowing the gas flow to be alternated over the sample from an oxidative to reductive atmosphere. The cell was designed for fluorescence XAS detection at high sample temperatures ($T_{max} \sim 800$ °C), while minimizing dead volume. A detailed description of this specially designed in situ XAS cell and the measuring diodes (I_0 and I_1) on the beamline can be found in the publication of Guilera et al. [14]. Throughout the sintering experiment, the pellet samples were heated to 800 °C under cyclic oxidizing/reducing conditions. Gas mixtures of 4 or 20% O_2 in He (150 cm^3/min) and 3% H_2 in He (150 cm^3/min) were introduced alternately into the cell every 60 s by using a gas-actuated switching valve. Mass spectra of the main gas components were measured by using Pfeiffer Ominstar quadrupole mass spectrometer. Pt L_{III}-edge XAS spectra were collected approximately every 6 s. Background subtraction and normalization were performed using the REX2000 program Ver.2.5.9 (Rigaku Corp.). Pt foil was used as a reference sample for accurate energy calibration of the XANES spectra.

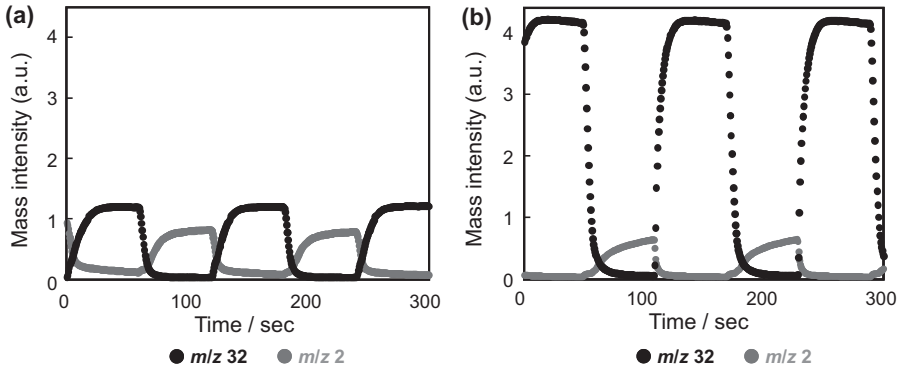

Fig. 1. Variations in the detected ion current of m/z 2 and m/z 32. (a) 4% O_2/3% H_2 cycling, (b) 20% O_2/3% H_2 cycling at room temperature.

3. Results and discussion

3.1. Structural characterization

Some basic characteristics of the catalysts prepared in this study are summarized in Table 1. CZY support has a cubic structure, and its specific surface area value is 99 m^2/g. The BET (Brunauer–Emmett–Teller) surface area of γ-type Al_2O_3 support (185 m^2/g) is higher than that of the CZY support. The BET surface areas of the CZY and Al_2O_3 supports after calcination at 800 °C for 3 h were 58 and 154 m^2/g, respectively. The high temperature treatment resulted in 40% decreases in the surface area of the CZY support. The Al_2O_3 support has a high thermal stability compared with the CZY support. The average size of Pt metal particles for these catalysts was estimated from XRD and the CO chemisorption method. No diffraction peaks from the Pt(1 1 1) could be detected in any of Pt/CZY and Pt/Al_2O_3 catalysts, because of their small particle size. This indicates that there are no large Pt metal particles in these samples. The same observation applies to the result of CO chemisorption method. The average Pt particle sizes in Pt/CZY and Pt/Al_2O_3 are about 1 nm, suggesting that the Pt particles after preparation are highly dispersed on the support. There was no change in the particle size on the loading amount of Pt supported on CZY.

3.2. Feasibility test of the experimental set-up for in situ T-XAS

To test the feasibility of in situ T-XAS experiment, we first checked the response of the gas switching in this system. Fig. 1 presents variations in the detected ion current of m/z 2 (H_2) and m/z 32 (O_2) in the outlet gas. 4 or 20% O_2/He (150 cm^3/min) and 3% H_2/He (150 cm^3/min) were introduced alternately into the cell every 60 s at room temperature. The gas flowing over the sample was quickly changed between an oxidative and reductive atmosphere.

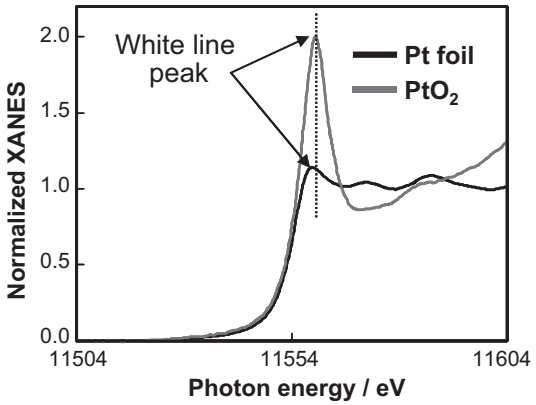

Fig. 2. Pt L_{III}-edge XANES spectra for standard samples of Pt foil and PtO_2 powder measured by Turbo-XAFS in fluorescence mode.

Next, Pt L_{III}-edge XANES spectra were collected using T-XAS in fluorescence mode. Normalized XANES spectra for standard samples of Pt foil and PtO_2 powder are shown in Fig. 2. The features present in these XANES spectra are in excellent agreement with those expected for these reference materials from a conventional scanning EXAFS experiment. The steeply rising absorption edge is referred to as the "white line." The white line of the Pt L_{III}-edge XANES arises from the electron transition of the $2p_{3/2}$ mainly to $5d_{5/2}$ and $5d_{3/2}$ orbitals. The contribution of the p–d orbital transition in the white line at L_{III}-edge is ca. 50 times stronger than that of p–s transition [15]. Since the absorption intensity of the white line reflects the vacancy in the 5d orbitals of Pt atoms, the white line intensity is expected to be an indication for the oxidation state of Pt. The intensity of the white line increases with the decreasing d-band occupancy, and a large white line intensity is observed on oxidized Pt such as PtO_2. In contrast, a small white

Table 1
The Catalyst samples, BET surface area and Pt particle size.

Catalyst[a]	Pt loading (wt%)	Support	BET surface area of support (m^2/g)	Pt particle size (nm)	
				XRD[d]	CO pulse
Pt/CZY	2	Ce–Zr–Y mixed oxide,[b] cubic-type	99 (58)[c]	ND[e]	1.1
Pt/CZY	1	↑	↑	ND[e]	1.1
Pt/CZY	0.5	↑	↑	ND[e]	1.0
Pt/Al_2O_3	2	γ-Al_2O_3	185 (154)[c]	ND[e]	1.0

[a] For sample description, see Section 2.
[b] Ce–Zr–Y mixed oxide contains 50 wt% CeO_2, 46 wt% ZrO_2 and 4 wt% Y_2O_3.
[c] The BET surface area after calcination at 800 °C for 3 h is given in the parentheses.
[d] The catalyst samples were reduced by 5% H_2 (N_2 balance) at 400 °C for 30 min before the XRD measurements. Average particle size was estimated from Pt(1 1 1) line width.
[e] The diffraction peak from the Pt particles could not be detected.

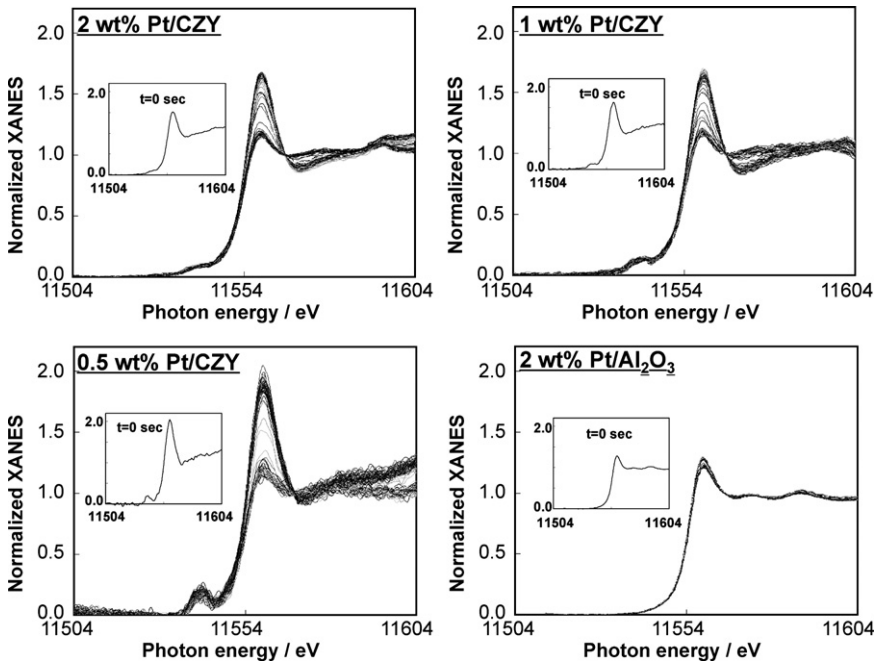

Fig. 3. Serial time-resolved Pt L_{III}-edge XANES spectra of Pt-supported catalysts under cyclical oxidizing/reducing condition. Spectra were collected approximately every 6 s. Variations in the first a hundred XANES spectra for 2, 1 and 0.5 wt% Pt/CZY and 2 wt% Pt/Al_2O_3 under oxidizing/reducing atmosphere at 800 °C in Fig. 4. Inset: the first XANES spectrum at the start (0 s) of the measurement.

line intensity is observed on reduced Pt such as Pt foil. Besides, the absorption energy at the top of the white line peak changed according to the Pt oxidation state. The peak top energy of white line for the Pt foil slightly shifted to low energy (ca. 1.0 eV), compared with the PtO_2. This energy shift in oxidation state is smaller than the actual natural width of the L_{III}-edge of Pt (5.31 eV) [16]. Therefore, the most obvious way to evaluate the change in oxidation state in our experiment is to look at the white line height due to the creation of electronic vacancies in the 5d orbital. Fig. 3 shows serial time-resolved XANES spectra of Pt-supported catalysts used in this study. Spectra were collected approximately every 6 s. These spectra give a variation in the first a hundred XANES spectra under cyclic oxidizing/reducing conditions at 800 °C, and correspond to the temporal dependence of the white line peak height in Fig. 4. This methodology of fluorescence T-XAS permitted continuous acquisition of XANES spectra of both Pt/Al_2O_3 and Pt/CZY (low-loaded Pt samples containing extremely absorbing matrixes). In this study, the quality was sufficient for measuring, after normalization, the height of the white line to study quantitatively the Pt sintering process. A weak peak is present just below the edge at around 11,540 eV, evident especially on the spectra for the 0.5 wt% Pt/CZY. In general, the pre-edge absorption, a shoulder peak below the rising absorption

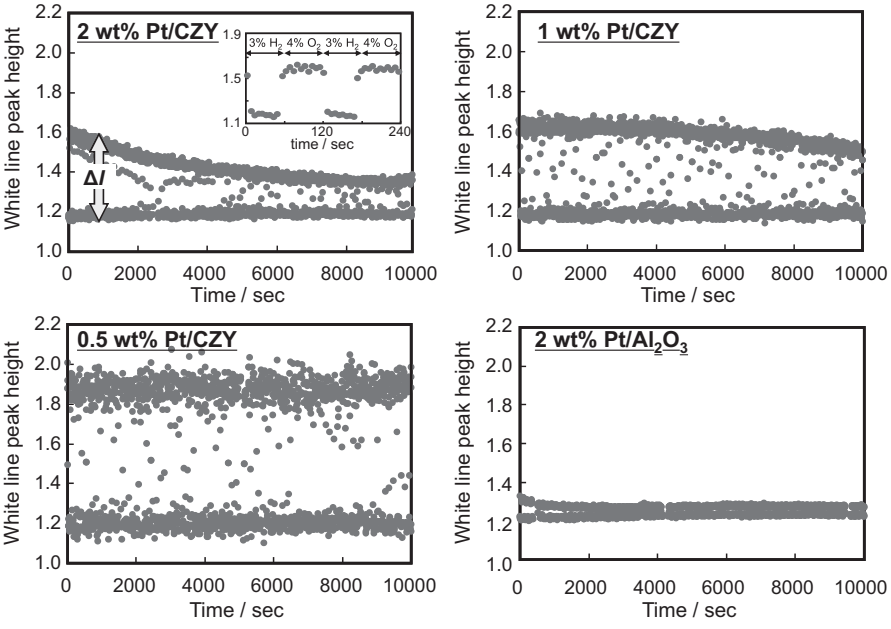

Fig. 4. Temporal dependence of the white line peak height of Pt L_{III}-edge XANES for 2, 1 and 0.5 wt% Pt/CZY and 2 wt% Pt/Al_2O_3. 4% O_2/He and 3% H_2/He gases were alternately introduced into the cell every 60 s at 800 °C. Inset: magnified view of initial stage of the experiment for 2 wt% Pt/CZY.

Table 2
ΔI and average Pt particle size for the Pt supported catalysts at 800 °C.

Catalyst	ΔI[a]		Average Pt particle size/nm[b]	
	Initial[c]	Final[c]	Initial[c]	Final[c]
2 wt% Pt/CZY	0.42 ± 0.03	0.17 ± 0.02	2.5	6.2
1 wt% Pt/CZY	0.45 ± 0.04	0.34 ± 0.04	2.3	3.1
0.5 wt% Pt/CZY	0.71 ± 0.09	0.72 ± 0.08	1.5	1.5
2 wt% Pt/Al_2O_3	0.12 ± 0.01	0.05 ± 0.01	8.7	21

[a] Difference between the white line peak height of the oxidized and reduced samples in Fig. 4.
[b] Pt particle size in diameter, estimated from the mean value of ΔI. For the correlation between the Pt particle size and ΔI, see Fig. S2 in the Supplementary data.
[c] Initial (0 s) and final (after 10,000 s) of the measurement at 800 °C under redox cycling.

edge, can be observed in K- or L_I-edge XANES, but not in Pt L_{III}-edge XANES [17,18]. Therefore, it is reasonable to suppose that this weak peak is due to factors other than Pt absorption. We assume that this weak peak comes from a glitch or a contamination of W (L_{II}-edge at 11,539 eV), but the precise origin of this unexpected peak is as yet not well known. However, this feature had almost no influence on the normalization of XANES spectra and the white line peak height. The white line peak height in these samples was changing during cyclic oxidizing/reducing conditions.

3.3. Sintering behavior of Pt particles

Fig. 4 shows the temporal change in the white line peak height of the normalized Pt L_{III}-edge XANES for the Pt/CZY and Pt/Al_2O_3 catalysts under cyclical oxidizing/reducing conditions at 800 °C. 4% O_2/He gas and 3% H_2/He gas were alternately introduced into the cell every 60 s. Pt L_{III}-edge XANES spectra were collected approximately every 6 s. The inset in Fig. 4 of 2 wt% Pt/CZY is the enlarged view in the first 240 s. Under a reductive atmosphere of 3% H_2/He, the supported Pt is in a metallic state and the white line peak is low. On the other hand, under oxidative atmosphere, the surface of Pt particles can be oxidized, and the white line peak is high. ΔI in Fig. 4 of 2 wt% Pt/CZY denotes the difference between the white line peak height of the oxidized and reduced samples. From a previous experiment, we found that the ΔI increased with the decreasing particle size of Pt [11,19]. This was confirmed by the relationship between the Pt particle size (Pt dispersion) measured by CO pulse adsorption method and ΔI [19]. An appropriate linear relationship between the two factors could be obtained. This suggests that the Pt particles are oxidized on the surface region, and that the portion of oxidized Pt atoms is proportional to the surface area of Pt particles. The detailed description of this ΔI method and the linear relationship can be found in Fig. S2 in the Supplementary data. Thus, using the correlation between the Pt particle size and ΔI, it is possible to track the change in average Pt particle size during in situ redox cycling.

Here, we must mention the white line peak height of the Pt metallic state under the reductive atmosphere. Vaarkamp et al. reported that the white line intensity of the Pt metallic state at Pt L_{III} and L_{II}-edge were affected by the particle size of Pt metal particles, and the changes in the intensity were larger for the L_{II}-edge [20]. The differences in the particle size of Pt metallic state have little influence on the white line peak height of Pt L_{III}-edge. Actually, in our case of quick scanning XANES at Pt L_{III}-edge, the white line peak height of the Pt metallic state under the reductive atmosphere was constant within a certain range. In addition, the variations of ΔI (the difference between the white line peak height of the oxidized and reduced samples) are much larger than the differences in the Pt metallic state. The ΔI method in this study is therefore sufficiently available to evaluate the Pt particle size.

In Fig. 4, the ΔI of 2 wt% Pt/CZY and 1 wt% Pt/CZY at 0 s were smaller than those of 0.5 wt% Pt/CZY and decreased with time. The ΔI of 2 wt% Pt/CZY decreased more rapidly than that of 1 wt% Pt/CZY. The ΔI of 0.5 wt% remained constant within the error bars until 10,000 s. On the other hand for the 2 wt% Pt/Al_2O_3 sample, the initial ΔI was significantly small compared to the 2 wt% Pt/CZY, and almost constant through the measurement. Using the correlation between the Pt particle size and ΔI, the average Pt particle sizes at the start (0 s) and at the end (after 10,000 s) of the measurement at 800 °C are summarized in Table 2.

The first point to be discussed is the support effect on the Pt sintering in Pt/CZY and Pt/Al_2O_3 with the same loading amount of 2 wt%. The average Pt particle size of the 2 wt% Pt/CZY increased from 2.5 to 6.2 nm. In contrast, the Pt particles in the 2 wt% Pt/Al_2O_3 already grew up to 8.7 nm in size when the measurement temperature went up to 800 °C, and then Pt sintering led to further growth (Pt particle size; >20 nm). Before this Pt sintering measurement, the Pt particle size in both Pt/CZY and Pt/Al_2O_3 estimated by CO pulse method was ca. 1 nm as shown in Table 1. The driving force behind this sintering inhibition of Pt on CZY is attributed to the strong Pt–oxide–ceria support interaction created under an oxidative atmosphere [7]. Generally, it is well known that PtO_2 decomposes to Pt metal under oxidizing conditions at around 600 °C and above according to the thermodynamic phase diagram [21]. Previous work has shown that the CZY support stabilizes a high-oxidation state of Pt even at 800 °C through the formation of the surface Pt–O–Ce anchor [7]. Pt sintering is therefore strongly curtailed. The Pt–O–Ce species are considered to be stabilized at a high concentration of O_2. Therefore, the effect of O_2 concentration under redox cycling on Pt sintering behavior in 2 wt% Pt/CZY was investigated. Fig. 5 compares the results of 4% O_2/3% H_2 cycling (the same data mentioned in Fig. 4), with those using 20% O_2/3% H_2 cycling. It is clear that an effective inhibition of Pt sintering in the Pt/CZY is achieved with increasing O_2 concentration under redox cycling. This result supports that the rigid Pt–O–Ce anchor is highly stabilized at high O_2 concentration. In contrast, since the interaction between Pt and Al_2O_3 is weak, that is, a rigid Pt anchor site cannot form, Pt particles transport across the surface of the Al_2O_3

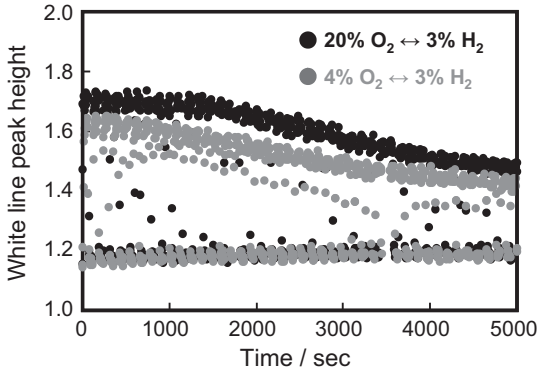

Fig. 5. Temporal dependence of the white line peak height of Pt L_{III}-edge XANES for 20% O_2/He and 3% H_2/He gases (●) and 4% O_2/He and 3% H_2/He gases (●) were alternately introduced into the cell every 60 s throughout the measurement.

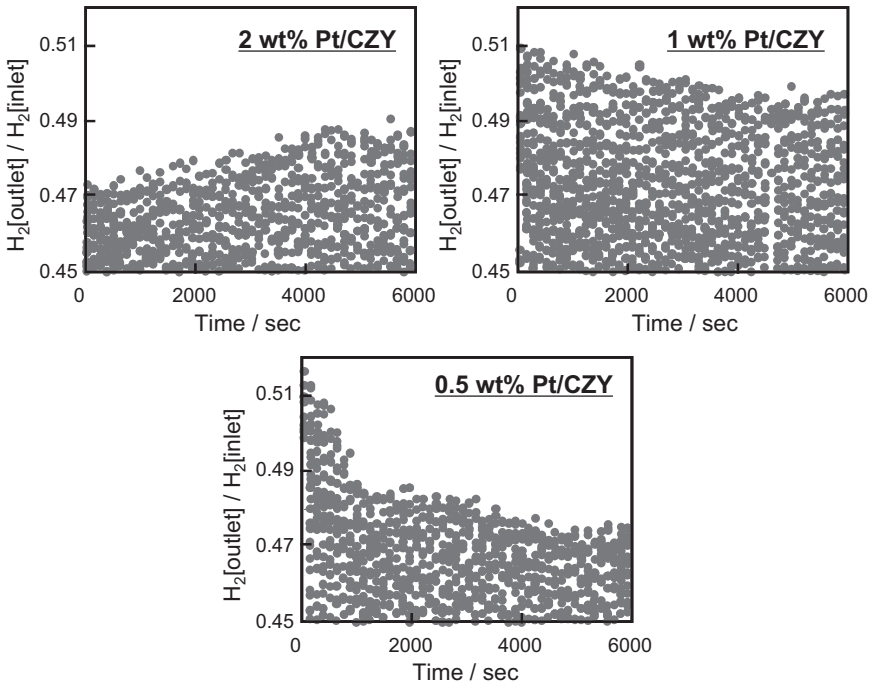

Fig. 6. Temporal dependence of the ratio of outlet to inlet H_2 (m/z 2) for 2, 1 and 0.5 wt% Pt/CZY catalysts. 4% O_2/He and 3% H_2/He gases were alternately introduced into the cell every 60 s at 800 °C.

support and easily sinter during a high temperature treatment. It is well known that the surface area of the support oxide has a considerable influence on Pt sintering [3]. The surface areas of the CZY and Al_2O_3 supports before this Pt sintering experiment are 99 and 185 m^2/g, respectively. In addition, the thermal stability of the CZY support is lower than that of the Al_2O_3 support (Table 1). Although the CZY has a markedly low surface area and the low thermal stability compared with the Al_2O_3, the CZY support has the effective ability to inhibit the Pt sintering. Therefore, the Pt–O–Ce anchor (i.e., the Pt–oxide support interaction) is the main factor of the sintering inhibition of Pt particles supported on CZY during the high-temperature redox aging.

The second point to be discussed is the loading amount of Pt supported on CZY. This Pt anchor effect in Pt/CZY catalyst appeared predominantly in the 1 and 0.5 wt% Pt/CZY, i.e. at lower loading amount of Pt. ΔI of the 1 wt% Pt/CZY in Fig. 4 decreased slowly in comparison with the 2 % Pt/CZY. The Pt particle size of the 1 wt% Pt/CZY slightly increased from 2.3 to 3.1 nm. It is noteworthy that ΔI of the 0.5 wt% Pt/CZY in Fig. 4 is maintained virtually constant, and the value of ΔI is large, suggesting that the Pt particles in the 0.5 wt% Pt/CZY remained highly dispersed. The Pt particle size of 1.5 nm in the 0.5 wt% Pt/CZY after 10,000 s was the same as that at the start of the measurement. Based on our observation above, an optimum amount of Pt loading could exist for the effective inhibition of Pt sintering, corresponding to the Pt anchor site on the surface of ceria-based oxide supports. Recently, a quantitative investigation of the optimum Pt loading to stabilize Pt atoms through Pt–O–Ce bond formation in Pt/ceria-based catalysts was reported by Hatanaka et al. [22], who stated that "catalysts with a lower Pt loading exhibited less catalytic deactivation and Pt sintering. The ideal Pt loading has an upper limit at both the catalytic activity and Pt particle size of aged catalysts. This upper limit was 0.25 g of Pt for 100 g of Ce–Zr–La–Pr mixed oxide. Based on the structure and composition around Pt on the ceria-based oxide, it was predicted that 5 Ce atoms on average interact with one Pt atom to form a Pt anchor site." The structure and composition of the forementioned Ce–Zr–La–Pr mixed oxide is very similar to the CZY support in this study. Since the upper limit of the Pt anchor site depends on an aging temperature, atmosphere and endurance time, a value of 0.25 g of Pt is not directly applied to that in our study. However, if this value could be used as an indication, 2 wt% and 1 wt% Pt would far exceed the value of 0.25 g Pt. Therefore, it is considered that the number of Pt anchor sites has an important role in the sintering of Pt particles on ceria-based oxide under redox cycling. It may be worth mentioning, in passing, that an induction period of Pt sintering is observed for the in the 1 wt% Pt/CZY (Fig. 4). The ΔI curve is almost constant until 4000 s, and then the Pt sintering begins to occur gradually. This Pt sintering behavior seems to have a close relation to the number of Pt anchor site. The effective anchor sites to inhibit the Pt sintering would decrease as the surface area of CZY support decreases during the thermal treatment. In other words, the CZY support has enough number of anchor sites to stabilize 1 wt% of Pt until 4000 s, and then the Pt aggregation would start, due to the lack of Pt anchor site with decreasing surface area of the CZY support. The above discussion includes speculation, because we have no definite information on the temporal dependence of surface area of the CZY support during thermal treatment. Further investigation is required to estimate the general validity.

3.4. Oxygen storage/release behavior of ceria–zirconia mixed oxide

It is well known that ceria oxide and CeO_2–ZrO_2 mixed oxide are widely used as a promoters due to their high oxygen storage/release capacity (OSC) based on the reversible redox Ce^{4+}/Ce^{3+} reaction ($CeO_2 \leftrightarrow CeO_{2-x} + (x/2)O_2$; $x = 0$–0.5) [23,24]. Ceria stores oxygen under oxygen excess conditions and releases it under oxygen deficient conditions in order to maintain the stoichiometric conditions. In this current set-up of the in situ T-XAS experiment, not only the XANES spectra, but online mass spectra of the gas species are simultaneously measured. Therefore, we can evaluate the OSC performance of the Pt/CZY catalyst during the Pt sintering measurement. Fig. 6 presents the temporal dependence of the ratio of outlet to inlet H_2 (m/z 2) during the redox cycling of the Pt sin-

tering measurement. The time scales in Fig. 6 correspond to those in Fig. 4. The concentration of inlet 3% H_2 gas under reductive condition of redox cycling is constant. Since H_2 species are oxidized on the catalyst surface by oxygen released from ceria oxide, the lower values of this ratio (outlet to inlet H_2) indicate the better OSC performance.

It has been reported that oxygen storage/release process on the Pt/ceria-based oxide mainly involves 3 steps: (1) reaction on the Pt surface, (2) oxygen surface diffusion on the ceria oxide and (3) oxygen bulk diffusion into the ceria oxide, and that Pt on the ceria oxide support promotes the process of oxygen storage and release [25,26]. In addition, Dong et al. reported that a smaller Pt particle size in Pt/CZY catalyst showed higher OSC performance in CO oxidation reaction [25]. In this study, the Pt sintering for 2 wt% and 1 wt% Pt/CZY occurred, whereas highly dispersed Pt particles in 0.5 wt% Pt/CZY were maintained. From these remarks, it was expected that the OSC performance of 2 wt% and 1 wt% Pt/CZY gradually got worse, and the 0.5 wt% Pt maintained the same performance. However, the results of the experiment were somewhat different from what had been anticipated. In Fig. 6, the OSC performance in 2 wt% Pt/CZY slightly dropped, while in 1 wt% Pt/CZY it got somewhat better, and in the 0.5 wt% sample it clearly improved. It is reasonable to suppose that the degradation of the OSC performance in the 2 wt% Pt/CZY would be mainly attributed to Pt sintering. However, the improved OSC of 1 wt% and 0.5 wt% Pt/CZY is incomprehensible. Several groups showed that a high temperature reductive treatment followed by a mild oxidation strongly modifies the oxygen release behavior of the CeO_2–ZrO_2 mixed oxide because a pyrochlore-type $Ce_2Zr_2O_7$ forms by the high temperature reduction of CeO_2–ZrO_2 which possesses an ordered arrangement of Ce and Zr ions [23,27,28]. Similarly, in the current experiment, it is possible to enhance the OSC performance by high temperature reduction during the redox cycling at 800 °C. Therefore, it is anticipated that the "apparent" OSC performance is not only affected by Pt particle size but also by the "intrinsic" factor in the bulk of CZY oxide. If this speculation is correct, the changes in the OSC performance of the 1 wt% and 0.5 wt% Pt/CZY catalysts are interpreted as follows. In the case of 1 wt% Pt/CZY, the Pt particle size increases but OSC enhancement due to intrinsic factors surpasses the Pt sintering effect. Since the Pt particles in the 0.5 wt% Pt/CZY remain highly dispersed, the improvement of the inherent OSC performance becomes available. However, this discussion, due to the lack of knowledge of the intrinsic factor in the CZY bulk, remains a matter of debate. In the current experiment, we estimated the apparent OSC by the mass measurement of outlet H_2 gas, but the level of Ce reduction during the oxygen release process, that is the intrinsic OSC of CZY oxide, was not quantified. A Ce K-edge XANES measurement could make it possible to directly evaluate the intrinsic OSC of CZY oxide. The combination of Ce K-edge measurement for the inherent OSC, Pt L_{III}-edge measurement for the Pt particle size and online mass spectrometry for the apparent catalytic performance must clarify the whole picture of the degradation in the TWCs. We plan to make the foregoing comprehensive investigation.

4. Conclusion

We have exploited the Turbo-XAS technique in fluorescence mode to perform in situ real time observation of Pt sintering process for Pt supported on CZY and Al_2O_3 supports under cyclic oxidizing/reducing conditions at 800 °C. The influence of support oxide and Pt loading amount on Pt sintering was investigated. We measured the white line peak height of Pt L_{III}-edge XANES, together with online mass spectrometry for the evaluation of the oxygen storage/release (OSC) performance under cyclic redox conditions at 800 °C. The results obtained are as follows:

(a) The sintering of Pt particles in 2 wt% Pt/ceria-based oxide could be inhibited under redox cycling at 800 °C, when compared to in 2 wt% Pt/Al_2O_3. In addition, Pt sintering in the Pt/CZY is achieved with increasing O_2 concentration under redox cycling. We proposed that the strong Pt–O–Ce anchor site in the Pt/CZY under the oxidizing condition during redox cycling causes the stabilization of high-oxidation state of Pt and the inhibition of Pt sintering.
(b) We found that 0.5 wt% Pt and 1 wt% Pt/ceria-based oxide with a lower Pt loading brought higher stability of Pt against sintering. Especially, the Pt particles in the 0.5 wt% Pt/CZY remained highly dispersed. The Pt particle size of 1.5 nm in the 0.5 wt% Pt/CZY after 10,000 s was the same as that at the start of the measurement. The Pt anchor site (its strength and number) has an important role in the sintering inhibition of Pt particles on CZY under cyclic redox conditions.
(c) The OSC performance in 2 wt% Pt/CZY slightly dropped, while in 1 wt% Pt/CZY it got somewhat better, and in the 0.5 wt% sample it clearly improved. It is presumed that these changes in OSC performance depend on not only Pt particle size but also the intrinsic factor in the bulk of CZY oxide.

Finally, through this research, we have determined an important guide that catalyst design at the atomic level is necessary in order to develop high performance and longevity catalysts for practical use.

Acknowledgements

The authors are grateful to Bernard Gorges, Olivier Mathon, Sebastien Pasternak, Florian Perrin, Steven Fiddy (ESRF), Muriel Lepage, Takashi Kuzuya (TOYOTA Motor Europe), Takamasa Nonaka, Satoshi Yamaguchi, Yoshiki Seno (TOYOTA Central R&D), Takeshi Hirabayashi and Masahide Miura (TOYOTA Motor corporation) for their excellent work.

Appendix A. Supplementary data

Supplementary data associated with this article can be found, in the online version, at doi:10.1016/j.cattod.2011.02.046.

References

[1] S. Matsumoto, Catal. Today 90 (2004) 183.
[2] P.J.F. Harris, J. Catal. 97 (1986) 527.
[3] R.M.J. Fiedorow, B.S. Chahar, S.E. Wanke, J. Catal. 51 (1978) 193.
[4] C.H. Bartholomew, Appl. Catal. A 212 (2001) 17.
[5] H. Birgersson, L. Eriksson, M. Boutonnet, S.G. Järås, Appl. Catal. B 54 (2004) 193.
[6] R.A. Dalla Betta, R.C. McCune, J.W. Sprys, Ind. Eng. Chem., Prod. Res. Dev. 15 (1976) 169.
[7] Y. Nagai, T. Hirabayashi, K. Dohmae, N. Takagi, T. Minami, H. Shinjoh, S. Matsumoto, J. Catal. 242 (2006) 103.
[8] A.F. Diwell, R.R. Rajaram, H.A. Shaw, T.J. Truex, Stud. Surf. Sci. Catal. 71 (2001) 139.
[9] L.L. Murrell, S.J. Tauster, D.R. Anderson, Stud. Surf. Sci. Catal. 71 (2001) 275.
[10] S. Pascarelli, T. Neisius, S. De Panfilis, J. Synchrotron Rad. 6 (1999) 1044.
[11] Y. Nagai, N. Takagi, Y. Ikeda, K. Dohmae, T. Tanabe, G. Guilera, S. Pascarelli, M. Newton, H. Shinjoh, S. Matsumoto, AIP Conf. Proc. 882 (2007) 594.
[12] T. Uchijima, Catalytic Science and Technology, Kodansha-VCH, Weinheim, 1990.
[13] T. Tanabe, Y. Nagai, T. Hirabayashi, N. Takagi, K. Dohmae, N. Takahashi, S. Matsumoto, H. Shinjoh, J.N. Kondo, J.C. Schouten, H.H. Brongersma, Appl. Catal. A 370 (2009) 108.
[14] G. Guilera, B. Gorges, S. Pascarelli, H. Vitoux, M.A. Newton, C. Prestipino, Y. Nagai, N. Hara, J. Synchrotron Rad. 16 (2009) 628.
[15] B.K. Teo, P.A. Lee, J. Am. Chem. Soc. 101 (1979) 2815.
[16] M.O. Krause, J.H. Oliver, J. Phys. Chem. Ref. Data 8 (1979) 329.
[17] T. Yamamoto, X-ray Spectrom. 37 (2008) 572.
[18] A.N. Mansour, J.W. Cook, D.E. Sayers, J. Phys. Chem. 88 (1984) 2330.
[19] Y. Nagai, K. Dohmae, Y. Ikeda, N. Takagi, T. Tanabe, N. Hara, G. Guilera, S. Pascarelli, M.A. Newton, O. Kuno, H. Jiang, H. Shinjoh, S. Matsumoto, Angew. Chem., Int. Ed. 47 (2008) 9303.

[20] M. Vaarkamp, J.T. Miller, F.S. Modica, G.S. Lane, D.C. Koningsberger, Stud. Surf. Sci. Catal. 75 (1993) 809.
[21] S.E. Livingstone, Pergamon Text in Inorganic Chemistry 25 (1973).
[22] M. Hatanaka, N. Takahashi, T. Tanabe, Y. Nagai, K. Dohmae, Y. Aoki, T. Yoshida, H. Shinjoh, Appl. Catal. B 99 (2010) 336.
[23] Y. Nagai, T. Yamamoto, T. Tanaka, S. Yoshida, T. Nonaka, T. Okamoto, A. Suda, M. Sugiura, Catal. Today 74 (2002) 225.
[24] Y. Nagai, K. Dohmae, K. Teramura, T. Tanaka, G. Guilera, K. Kato, M. Nomura, H. Shinjoh, S. Matsumoto, Catal. Today 145 (2009) 279.
[25] F. Dong, T. Tanabe, A. Suda, N. Takahashi, H. Sobukawa, H. Shinjoh, Chem. Eng. Sci. 63 (2008) 5020.
[26] A. Suda, K. Yamamura, H. Sobukawa, Y. Ukyo, T. Tanabe, Y. Nagai, F. Dong, M. Sugiura, J. Ceram. Soc. Jpn. 112 (2004) 623.
[27] T. Omata, H. Kishimoto, S. Otsuka-Yao-Matsuo, N. Ohtori, N. Umesaki, J. Solid. State Chem. 147 (1999) 573.
[28] P. Fornasiero, R. Di Monte, G. Rao Ranga, J. Kašpar, S. Meriani, A. Trovarelli, M. Granziani, J. Catal. 151 (1995) 168.